RSC Advances

PAPER

View Article Online
View Journal | View Issue

Cite this: *RSC Adv.*, 2024, **14**, 15821

Antibacterial efficacy of copper-based metal–organic frameworks against *Escherichia coli* and *Lactobacillus*

Sandy Elmehrath, [ab] Khansa Ahsan, [a] Nayla Munawar, [a] Ahmed Alzamly, [a] Ha L. Nguyen [c] and Yaser Greish [*ad]

The widespread and excessive use of antimicrobial drugs has resulted in a concerning rise in bacterial resistance, leading to a risk of untreatable infections. The aim of this study was to formulate a robust and efficient antibacterial treatment to address this challenge. Previous work focused on the effectiveness of the Cu-BTC metal–organic framework (MOF; BTC stands for 1,3,5-benzenetricarboxylate) in combatting various bacterial strains. Herein, we compare the antibacterial properties of Cu-BTC with our newly designed Cu-GA MOF, consisting of copper ions bridged by deprotonated gallate ligands (H_2gal^{2-}), against *Escherichia coli* (*E. coli*) and *Lactobacillus* bacteria. Cu-GA was synthesized hydrothermally from copper salt and naturally derived gallic acid (H_4gal) and characterized for antibacterial evaluation. The gradual breakdown of Cu(H_2gal) resulted in a significant antibacterial effect that is due to the release of copper ions and gallate ligands from the framework. Both copper MOFs were nontoxic to bacteria at low concentrations and growth was completely inhibited at high concentrations when treated with Cu-BTC (1500 μg for *E. coli* and 1700 μg for *Lactobacillus*) and Cu-GA (2000 μg for both bacterial strains). Furthermore, our agarose gel electrophoresis results indicate that both MOFs could disrupt bacterial cell membranes, hindering the synthesis of DNA. These findings confirm the antibacterial properties of Cu-BTC and the successful internalization of Cu^{2+} ions and gallic acid by bacteria from the Cu-GA MOF framework, suggesting the potential for a sustained and effective therapeutic approach against pathogenic microorganisms.

Received 18th February 2024
Accepted 8th May 2024

DOI: 10.1039/d4ra01241k

rsc.li/rsc-advances

Introduction

Metal–organic frameworks (MOFs) are constructed by coordinating metal ions or secondary building units (SBUs) with organic linkers, forming strong bonds with some degree of flexibility. These materials possess unique properties, such as defined networks, designability, ultrahigh porosity and surface areas that can reach up to 10 000 $m^2\ g^{-1}$.[1] Due to their remarkable features, MOFs have been extensively studied in various fields, including catalysis,[2] drug delivery,[3,4] sensing,[5,6] gas storage and separation[7,8] and imaging.[9,10] Further, bioMOFs that contain endogenous metal units coordinated with functional molecules such as amino acids, peptides, nucleobases, or saccharides, can be employed as pro-drugs in the treatment of various diseases and infections.[11–13] When used against certain bacterial strains, MOFs exhibit improved bacterial internalization, high selectivity and controlled release, thereby offering a viable alternative to traditional antibiotic utilization.

Antibiotic resistance is swiftly becoming a significant public health concern due to unnecessary and excessive use of antibiotics in recent years.[14,15] In the absence of effective alternatives, bacterial infections may once again become untreatable if resistance persists.[15,16] Bacteria can acquire resistance through a variety of mechanisms, rendering conventional antibiotics ineffective.[17] MOFs, when employed against specific bacterial strains, demonstrate enhanced bacterial internalization, remarkable selectivity, and regulated release of antibacterial reagents. As a result, they can serve as a substitute for conventional antibiotics. Moreover, combining imaging with new therapies provides a real-time monitoring of the pathological condition and treatment progress, offering guidance on exploring new medicines which can enhance treatment strategies to overcome the antibiotic resistance of existing conventional antibiotics.[18]

Since 1962, the research on copper's antimicrobial properties has been growing.[19] Multiple studies have demonstrated its effectiveness against various bacteria, including *Staphylococcus aureus* (*S. aureus*), *Clostridium difficile*, *Bacillus subtilis*, *Escherichia coli* (*E. coli*), *Pseudomonas aeruginosa* and *Legionella*

[a]*Department of Chemistry, United Arab Emirates University, Al-Ain, 15551, UAE. E-mail: y.afifi@uaeu.ac.ae*

[b]*Wyss Institute at Harvard University, Boston, MA, 02215, USA*

[c]*Department of Chemistry, University of California Berkeley, Berkeley, CA, 94720, USA*

[d]*Zayed Centre for Health Sciences, United Arab Emirates University, Al-Ain, 15551, UAE*

pneumophilia.[20–29] Binding to lipopolysaccharides, peptidoglycans, or carboxylic groups of bacteria, Cu^{2+} ions have been found to cause damage by disrupting the bacterial envelope.[30–33] This disruption is brought about by membrane depolarization due to the binding of Cu^{2+} ions to negatively charged domains, leading to a reduction in potential. Ultimately, this process may result in membrane leakiness or even complete rupture.[34] Bacterial cell damage can also be induced by the internalization or binding of Cu nanoparticles (NPs) by bacteria. Further, reactive oxygen species (ROS) generated by Cu NPs can lead to oxidative stress, eventually leading to deoxyribonucleic acid (DNA) damage and lipid peroxidation in bacterial membrane.[35–37]

Rodríguez *et al.* conducted a study to examine the antibacterial properties of HKUST-1. By attaching the MOF material to cellulosic fibers, the researchers discovered that it effectively hindered the growth of *E. coli*. They concluded that HKUST-1, not its individual constituents, was responsible for the antibacterial activity against *E. coli*.[38] Additionally, previous research delved into the antimicrobial potency of Cu-BTC (another name of HKUST-1; BTC = 1,3,5-benzenetricarboxylate) against *E. coli* and *S. aureus*. Results demonstrated that the MOF material exhibited the ability to hinder bacterial growth at elevated concentrations (900 mg L^{-1} for *E. coli* and 1200 mg L^{-1} for *S. aureus*), which caused cytoplasm and flagella damage to the bacteria. Cu-BTC treatment also induced oxidative stress, resulting in further impairment to the membrane and DNA.[39,40]

Gallic acid (H_4gal) or 3,4,5-trihydroxybenzoic acid, is a phenolic compound that exhibits anti-inflammatory,[41] anti-carcinogenic,[42] antimicrobial,[43] antifungal[44] and antioxidant[45] properties. Studies have demonstrated that H_4gal can disrupt the integrity of the cell membrane and inhibit the motility of several bacteria and biofilm,[43,46–48] leading to disintegration of the cell membrane and leakage of intracellular bacterial constituents and thus contributing to its antimicrobial effect.[49,50] Apart from its antimicrobial properties, H_4gal can also function as a pro-oxidant by producing ROS, leading to oxidative stress in cells.[50] Wang *et al.* improved the antimicrobial efficacy of H_4gal against *E. coli* O157:H7 by subjecting it to UV-A light for photo-irradiation. They discovered that the UV-A light enhanced the internalization of H_4gal into the bacteria allowing for increased ROS accumulation and oxidative damage to cells.[51] H_4gal has also been shown to inhibit the activity of bacterial dihydrofolate reductase and affect DNA cleavage in various bacterial strains.[52] However, H_4gal's efficacy is limited due to its poor bioavailability and rapid metabolism after digestion.[53] The goal is to increase absorption, reduce the elimination rate and improve the overall bioavailability of H_4gal. This work examines the antibacterial effects of Cu-BTC and Cu-GA MOFs on *E. coli* (Gram-negative) and *Lactobacillus* (Gram-positive) bacterial strains. Incorporating Cu^{2+} and gallate (H_2gal^{2-}) within a MOF framework offers the advantage of achieving a regulated and prolonged release of both constituents, in contrast to the unrestricted release that occurs with free copper and H_4gal. Cu-BTC has been utilized in various applications due to its high porosity and unique structural composition. However, Cu-GA is a newly developed MOF that hasn't been examined for its antibacterial properties. The metal unit in a MOF structure is crucial for bacterial inhibition, and the gallic acid linker may enable specific treatment of bacteria. Therefore, the antibacterial properties of the distinct MOFs in this study underline the potential for developing customized nanoparticles for inhibiting specific bacterial strains.

Experimental procedures

Materials

Copper(II) nitrate hemipentahydrate ($CuN_2O_6 \cdot 2.5H_2O$), and 1,3,5-benzenetricarboxylic acid (H_3BTC) were purchased from Sigma-Aldrich. *N*,*N*-dimethylformamide (DMF), dichloromethane, and ethanol were purchased from Fisher. Gallic acid monohydrate ($C_7H_6O_5 \cdot H_2O$) was purchased from Riedel-de Haën. Ultrapure water was obtained from a Millipore pure water system. All chemicals were used without further purification.

For the antibacterial evaluation experiments, nutrient broth and nutrient agar (Lab M Limited, United Kingdom), agarose (Sigma), and bacterial genomic DNA isolation Kit (abcam, United Kingdom) were obtained. Two strains of bacteria were used for the evaluation experiments: *E. coli* BL21 Strategene, USA and *Lactobacillus* – isolated from commercial grade prebiotic sachet.

Synthesis of MOF materials

To synthesize Cu-BTC, 1.0 g (4.76 mmol) of H_3BTC and 1.72 g (8.62 mmol) of copper(II) nitrate hemipentahydrate were dissolved in 24 mL of solvent consisting of equal parts DMF, ethanol, and deionized water. The mixture was transferred to a sealed tube and heated at 85 °C for 24 h. The resulting product was subjected to solvent exchange using dichloromethane and further activated at 140 °C for 24 h to remove any residual solvents and to evacuate the pores. Cu-GA MOF was prepared by dissolving gallic acid monohydrate (0.376 g, 2 mmol) in 5 mL of solvent consisting of equal parts of DMF, ethanol, and water. Then, copper(II) nitrate hemipentahydrate (0.232 g, 1 mmol) was also dissolved in 5 mL equal parts of DMF, ethanol, and water. Once the two solutions were completely dissolved, the copper solution was then added dropwise to the gallic acid solution while stirring. 5 M KOH was added to the Cu-GA mixture dropwise until the pH reached ~6.5. The reaction mixture was put in a sealed Teflon lined autoclave reactor and placed in the oven for 12 h at 120 °C. The sample was then washed with methanol 3 times daily for 2 days and then with DCM 3 times for 1 day for the evacuation of the original solvent from the pores.

Characterization of MOF materials

The morphology and particle size of the MOF samples were obtained using a JEOL JSM-6010LA scanning electron microscope (SEM). Powder X-ray diffraction (XRD) data was recorded on a Shimadzu-6100 powder XRD diffractometer with Cu-Kα radiation, $\lambda = 1.542$ Å. Thermogravimetric analysis (TGA) was

performed to determine the thermostability of the material. A Shimadzu DTG60 thermogravimetric analyzer with a temperature ramp of 10 °C min^{-1} in N_2 was used. Fourier transform infrared (FTIR) spectra (4000–400 cm^{-1}) were obtained from KBr pellets using a Bruker Vector 22 instrument.

Zone of inhibition

The antimicrobial efficacy of Cu-BTC and Cu-GA against *E. coli* BL21 (DE3) and *Lactobacillus* was evaluated using the standard zone of inhibition or dynamic contact method (ASTM E2149-13a) with slight modifications.[54] Initially, fresh inoculum containing 100 μL (approximately 1×10^5 CFU mL^{-1}) of *E. coli* and *Lactobacillus* cells were spread uniformly on Luria Bertani (LB) agar plates to create a smooth bacterial lawn. A 1 cm MOF disk was placed directly in the center of the plate and the antibacterial properties of the MOF were monitored after incubating the plates for 12, 24, and 48 h at 37 °C. Copper(II) acetate and H_4gal disks of similar size were used as controls. The diameter of the non-growth zone surrounding the MOF disk was measured in millimeters for each sample and a graph was plotted to depict the correlation between the incubation period and the inhibition zone.

Elucidation of the minimum inhibitory concentration (MIC)

In order to determine the minimum concentration of Cu-BTC and Cu-GA required to impede the growth of *E. coli* and *Lactobacillus* strains, the MIC was measured using the microtiter broth dilution technique.[55,56] A bacterial suspension of 5 μL, with a final concentration of 1×10^5 CFU mL^{-1}, was prepared in LB broth and added to each well of a 96-well plate. Each MOF was then subjected to two-fold dilution in the wells ranging in concentration from 7.81 μg to 2 mg. The plates were then incubated at 37 °C for 24 h. A negative control lacking MOF powder was also evaluated for antibacterial activity. The wells were assessed for absorbance at a wavelength of 600 nm, and the MIC of both MOFs was determined based on the well in which neither bacterial strain exhibited visible growth.

Time kill assay

The bactericidal activity of Cu-BTC and Cu-GA over time was conducted on bacterial strains in accordance with previous reports.[57] Individual bacterial suspensions were prepared in sterile LB broth as inoculum (pre-culture) and were diluted to achieve a final concentration of 1×10^5 CFU mL^{-1}.1% of each bacterial pre-culture, along with 1 × MIC of Cu-BTC and Cu-GA, were added to sterile LB broth and incubated at 37 °C for 24 h with continuous shaking at 170 rpm. Aliquots of each bacterial suspension were taken at 2 h intervals, and the OD was measured using a spectrophotometer (Shimadzu, Japan) at a wavelength of 600 nm. A bacterial culture without the test sample was employed as a control.

Agarose gel electrophoresis for DNA disintegration

To assess cell death caused by Cu-BTC and Cu-GA, the destruction and disintegration of DNA was analyzed using agarose gel electrophoresis. *E. coli* and *Lactobacillus* were separately treated with various concentrations (ranging from 0 to 1.5 × MIC) of Cu-BTC and Cu-GA, and then incubated at 37 °C for 24 h. After 24 h, each sample was collected, centrifuged, and its DNA was extracted using a Wizard® Genomic DNA purification kit (Promega). The extracted DNA was quantified using a NanoDrop 2000 (Thermofisher, North America LLC, FL, USA), and qualified by agarose gel electrophoresis. Where 5 μL of each Cu-BTC and Cu-GA treated sample was mixed with 1.5 μL of loading dye and run through a 1% agarose gel.

Results and discussion

Cu-BTC was synthesized in a sealed tube using solvothermal methods in a solvent mixture comprising equal proportions of DMF, ethanol, and water. The resulting MOF displayed a turquoise blue color, transitioning to a dark blue crystalline powder upon activation in a vacuum oven. The Langmuir and the Brunauer–Emmett–Teller (BET) surface areas are 1507 m^2 g^{-1} and 1268.9 m^2 g^{-1}, respectively. The pore volume was 0.54 cm^3 g^{-1} and the pore size and width distribution obtained by Horvath–Kawazoe was about 57.86 Å and 7.6 Å, respectively. Cu-GA was synthesized hydrothermally in a Teflon-lined autoclave reactor, yielding a brown crystalline powder. Due to the highly agglomerated morphology of the Cu-GA flaky particulates, the MOF displayed weak adsorption of N_2, with an average pore size of 200 Å. The measured BET and Langmuir surface area values were of 1.41 and 4.23 m^2 g^{-1}, respectively.

The PXRD pattern of Cu-BTC shown in Fig. 1a indicates a high degree of crystallinity with intense peaks present within the 2θ range of 5° to 15°. Among these, the most prominent peaks were observed at 2θ values of 5.97, 6.88, 9.67, 11.80, and 13.58°. The PXRD pattern of the as-prepared Cu-GA MOF is shown in Fig. 1b, revealing a highly crystalline material with the most prominent peak at 10.3°. The SEM micrograph in Fig. 1c illustrates that Cu-BTC possesses a defect-free octahedral crystal structure with well-defined edges and a consistent morphology and size distribution. In contrast, Cu-GA appears as highly agglomerated 2D flakes with an average size of 1 μm and thickness of <1 μm (Fig. 1d). PXRD and SEM results for Cu-GA align with the findings from previously cited reports.[58,59]

Fig. 2 presents the FT-IR spectra and TGA thermograms for both Cu-BTC and Cu-GA MOFs, with the corresponding spectra of the pure linkers (H_3BTC and H_2gal^{2-}) included for comparison. Compared with the broad band extending between 2500 and 3250 cm^{-1} in the FT-IR spectrum of the BTC linker, the Cu-BTC spectrum showed a weak absorption at 3570 cm^{-1}, possibly indicating the presence of physically adsorbed water (I). Band shifts at 1693 cm^{-1} to 1639 cm^{-1} (C=O) and at 1454 and 1407 cm^{-1} to 1445 and 1378 cm^{-1} (C–O) indicate the complete

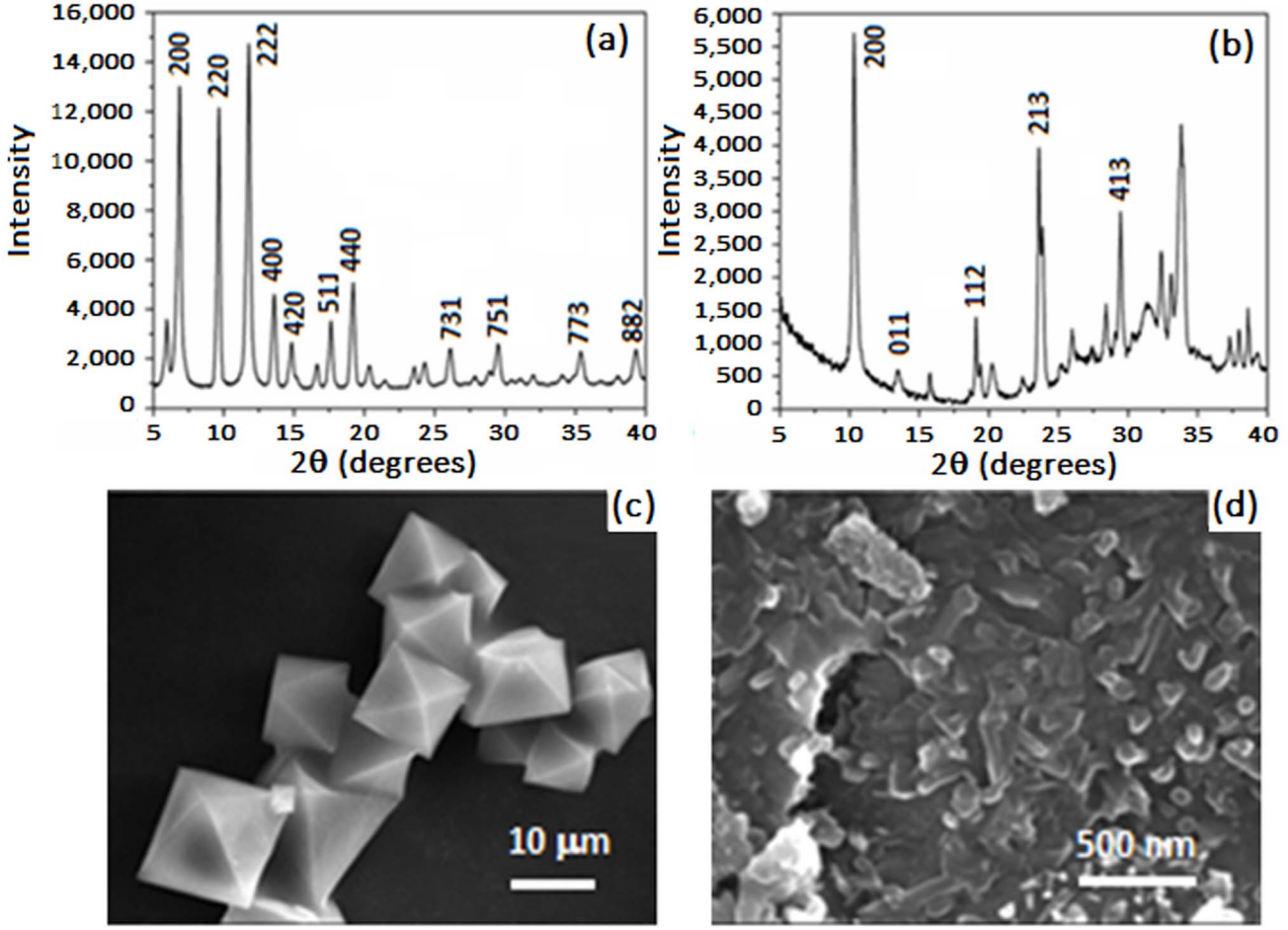

Fig. 1 PXRD spectrum and SEM images for Cu-BTC (a and c) and Cu-GA (b and d).

ionization of the BTC-COOH groups and the formation of the Cu-BTC structure (II). Both Cu-GA and the H_2gal^{2-} linker FT-IR spectra reveal the presence of a broad band at 3237 cm^{-1}, which is attributed to the unionized OH groups along the H_2gal^{2-} linker molecule. Three bands at 3482, 3370, and 3274 cm^{-1} are associated with the –COOH and –OH groups of the H_2gal^{2-} linker (I). Additionally, the variations in the intensities of the bands at 1444 cm^{-1} and 1027 cm^{-1} (O–H and C–O groups, respectively), confirm the formation of the Cu-GA MOF structure (II).[59]

The TGA thermograms depicted in Fig. 2c and d for the pure H_3BTC and H_2gal^{2-} linkers, respectively, reveal a continuous and gradual breakdown of these molecules. In Fig. 2c, the TGA curve of the pure H_3BTC linker exhibits two distinct thermal events around 350 and 450 °C (II and III), corresponding to the decarboxylation of the H_3BTC structure and the subsequent decomposition of the remaining aromatic ring of the H_3BTC molecule. The Cu-BTC TGA thermogram exhibits three thermal events. Alongside the decarboxylation and breakdown of the aromatic ring, an initial event (I) is observed, attributed to the removal of adsorbed water molecules around 150 °C.[60] The TGA curve of the H_2gal^{2-} linker shows the presence of three events attributed to the removal of water vapor around 150 °C and the gradual degradation of the structure at 300 and 350 °C. These events were followed by a slow rate of decomposition of the remaining aromatic ring between 350 and 600 °C. However, Cu-GA exhibited dihydroxylation and decarboxylation events alongside the gradual decomposition of the aromatic ring (II and III).[61] Observations also reveal that the final weight loss values for the Cu-BTC and Cu-GA structures were 70% and 55%, respectively. This suggests the presence of CuO residue as the remaining phase in both structures.

Both copper-based MOFs were tested for their antibacterial activity due to their high degree of crystallinity, biocompatibility, structured arrangement, and bactericidal properties of the metal ions contained within the framework. While Cu-GA may not provide as large a pore size as Cu-BTC, the stability of the ligand within the structure facilitates the gradual release of H_2gal^{2-}. Both MOFs were tested against *E. coli* (Gram negative) and *Lactobacillus* (Gram-positive) bacterial strains. The standard zone of inhibition test, a quantitative analysis of bacterial growth (ASTM E2149-13a), indicate an increasing diameter of a clear zone of inhibition around the sample disks after incubation with *E. coli* and *Lactobacillus* for 12, 24, and

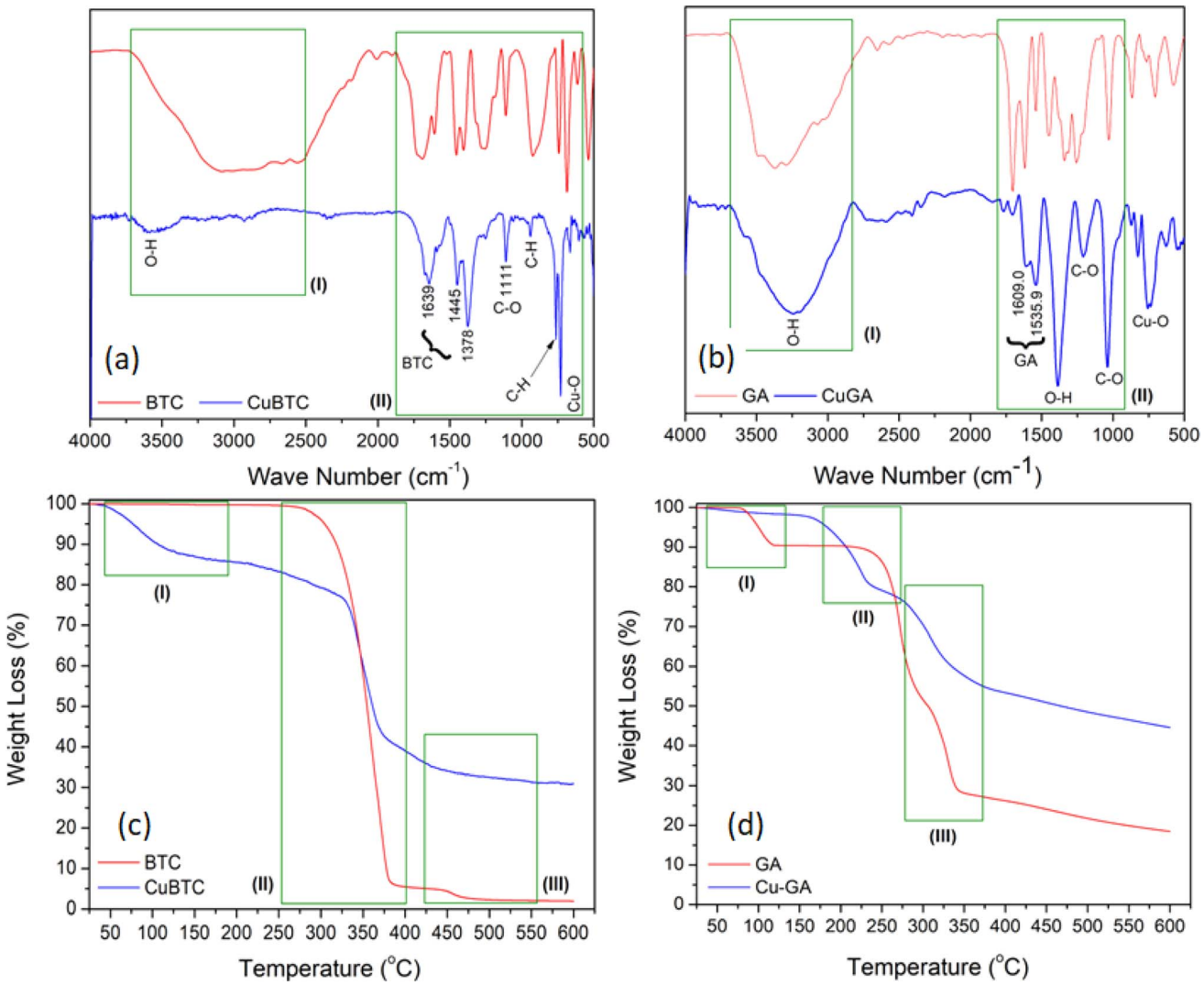

Fig. 2 FT-IR spectra and TGA-DTG profile for Cu-BTC (a and c) and Cu-GA (b and d). Profile of linkers included for comparison.

48 h (Fig. 3a and b). The larger inhibition zone observed with longer exposure time is attributed to the increased leaching of Cu^{2+} ions from both MOFs. Cu-BTC exhibited a 2 mm and 6.5 mm zone of inhibition with *E. coli* and *Lactobacillus*, respectively, at 12 h (Fig. 3c). In contrast, Cu-GA showed a wider zone of inhibition against *E. coli*, measuring 5.5 mm, but only exhibited a 1 mm zone of inhibition against *Lactobacillus* (Fig. 3d). At 48 h, Cu-BTC showed a 4 mm zone of inhibition against *E. coli*, while Cu-GA exhibited an impressive 17 mm zone (Fig. 3c and d). In addition, Cu-GA demonstrated a much larger zone of inhibition than Cu-BTC in *E. coli* at 24 h. H_4gal can compromise the cell membrane's integrity and hinder bacterial movement by producing ROS, leading to cellular oxidative stress. To demonstrate the inhibiting effect of both constituents in the MOF structures, copper(II) acetate and pure H_4gal were used as controls (Fig. 4a and b). The metal salt showed a 13 mm, 17 mm, and 23.5 mm zone of inhibition against *E. coli* at 12, 24, and 48 h, respectively (Fig. 4c). Similar results were observed with the *Lactobacillus* strain (Fig. 4d). The copper control exhibited larger zones of inhibition, indicating a burst release effect, in contrast to both MOF samples, which demonstrated a more sustained release of copper ions. Furthermore, H_4gal, the antioxidant, was utilized as a control and was able to inhibit both strains of bacteria. Cu-GA demonstrated a more significant antibacterial effect in comparison to H_4gal alone, as evidenced by the smaller zones of inhibition with *E. coli*. Compared to *E. coli*, *Lactobacillus* exhibited lower resistance to almost all samples except for Cu-GA.

As a Gram-positive bacterium, *Lactobacillus* does not have an outer membrane, which makes it more susceptible to foreign attacks through the cell wall.[62] Cu^{2+} ions have been found to cause damage to the cell wall and cell membrane by binding to lipopolysaccharides or peptidoglycans or carboxylic groups of bacteria, resulting in a disruption of the bacterial envelope.[30–33] Further, Cu^{2+} ions are also known to cause complete membrane

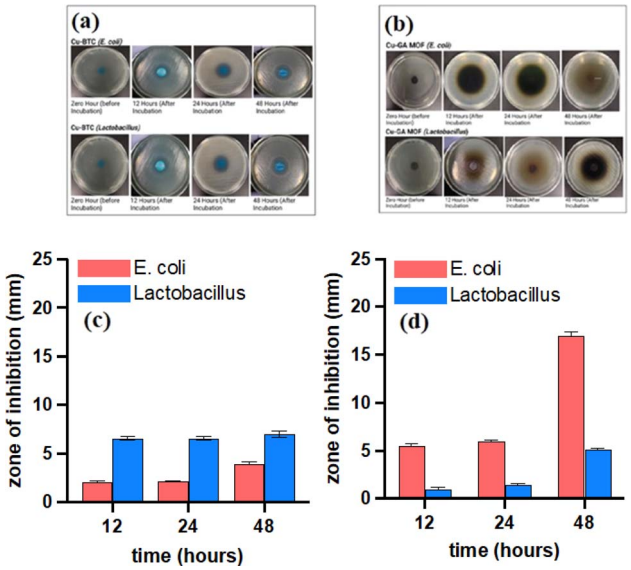

Fig. 3 Antibacterial activity and summary of zones of inhibition for Cu-BTC (a and c) and Cu-GA (b and d) MOFs against *E.coli* and *Lactobacillus* bacterial strands.

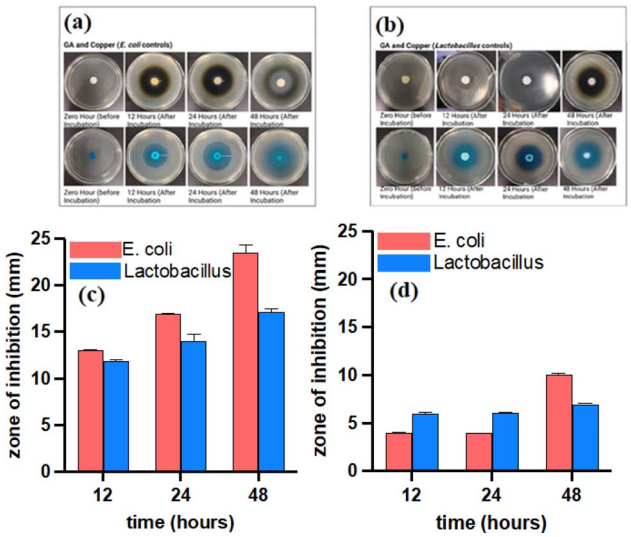

Fig. 4 Antibacterial activity for Cu^{2+} and gallic acid controls (a and b) and summary of zones of inhibition for Cu^{2+} (c) and gallic acid controls (d) against *E.coli* and *Lactobacillus* bacterial strands.

rupture by binding to negatively charged domains and reducing the potential.[34] When combined with gallate linkers, they can generate ROS, leading to oxidative stress in cells and inhibiting the motility of bacteria, thus creating a more pronounced antibacterial effect.[43,46–48,50] This has also been demonstrated with other MOFs that do not contain copper.[63]

Table 1 displays the MIC of Cu-BTC and Cu-GA against *E. coli* and *Lactobacillus* at different concentrations ranging from 7.81 μg to 2000 μg. The findings reveal that Cu-BTC had a more pronounced antibacterial effect on *E. coli* than on *Lactobacillus*, compared to the control groups. The MIC of Cu-BTC against *E. coli* and *Lactobacillus* was found to be 1500 μg and 1700 μg, respectively. On the other hand, Cu-GA showed partial inhibition of microbial growth at 1800 μg and 1900 μg concentrations, but complete antimicrobial activity was observed at 2000 μg for both strains, as evidenced by the absence of growth (cloudiness) in the well (Fig. 5a–d).

The time-kill assay was used to confirm the bactericidal effects of Cu-BTC and Cu-GA against *E. coli* and *Lactobacillus*. As depicted in Fig. 6a and b, the growth of both bacterial species was significantly impacted by Cu-BTC and Cu-GA. While the growth curve of the control samples showed an increase in cellular proliferation, the presence of Cu-BTC and Cu-GA at 1 *x* MIC substantially impeded bacterial growth. This observation underscores the remarkable bactericidal potential of both MOFs at this concentration, signifying their potential significance in managing the emergence of multidrug-resistant bacterial strains. However, further testing at concentrations equal to or less than half of the MIC is needed in order to elucidate dose- and time-dependent dynamics, allowing for a more comprehensive exploration of the time-kill profiles exhibited by both MOFs against the targeted bacterial strains.

Agarose gel electrophoresis was used to investigate the impact of Cu-BTC and Cu-GA on the DNA of *E. coli* and *Lactobacillus*. The results illustrated in Fig. 7a–d reveal a noticeable decrease in the size and brightness of the DNA band for samples treated with Cu-BTC, indicating the disruption of the DNA morphology and growth inhibition of both bacterial strains. The degree of disruption was found to increase with increasing concentrations of Cu-BTC MOF. These findings suggest that copper-based MOFs can not only affect the bacterial cell membrane and wall but can also cause morphological damage to their DNA structure. Moreover, the extent of this disruptive

Table 1 MIC of Cu-BTC and Cu-GA against *E. coli* and *Lactobacillus* strains

		Concentration (μg)										
MIC of Cu-BTC against tested bacteria												
Strain	Control	1000	1100	1200	1300	1400	1500	1600	1700	1800	1900	2000
E. coli	+++	+++	+++	++	+	+	—	—	—	—	—	—
Lactobacillus	+++	+++	+++	+++	+++	+++	++	++	—	—	—	—
MIC of Cu-GA against tested bacteria												
Strain	Control	1000	1100	1200	1300	1400	1500	1600	1700	1800	1900	2000
E. coli	+++	+++	+++	+++	+++	+++	+++	+++	+++	++	+	—
Lactobacillus	+++	+++	+++	+++	+++	+++	+++	+++	+++	+++	++	—

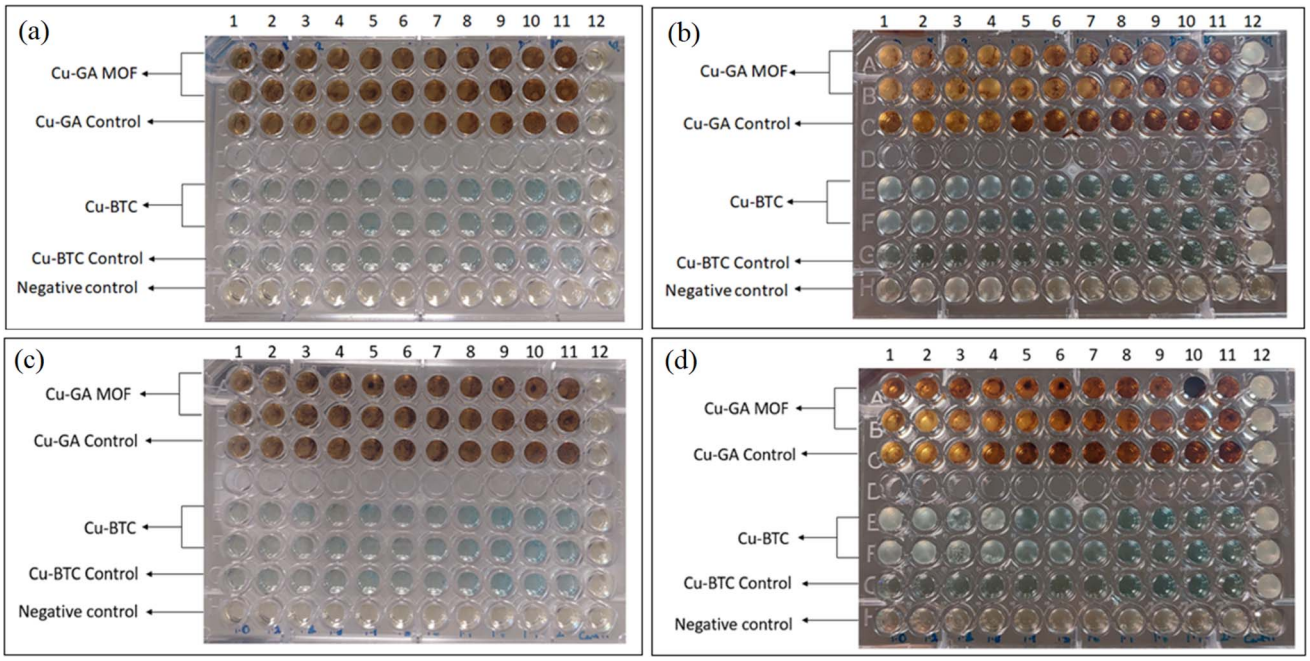

Fig. 5 MIC before incubation (a and c) and 24 h after incubation (b and d) of Cu-BTC and Cu-GA MOFs with *E. coli* (a and b) and *Lactobacillus* (c and d). (1) 1000 μg, (2) 1100 μg, (3) 1200 μg, (4) 1300 μg, (5) 1400 μg, (6) 1500 μg, (7) 1600 μg, (8) 1700 μg, (9) 1800 μg, (10): 1900 μg, (11) 2000 μg, (12): positive control *E. coli* (without MOF treatment).

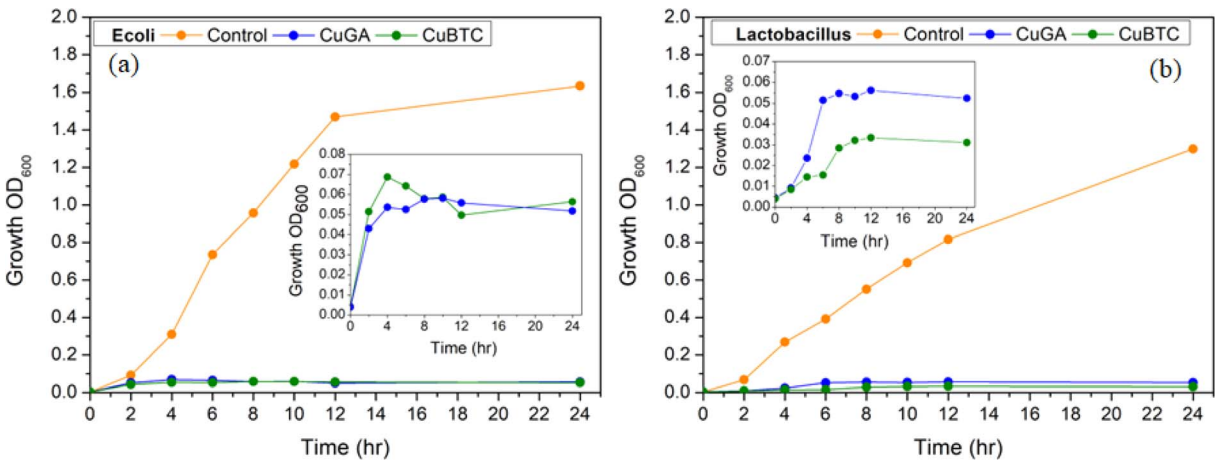

Fig. 6 Time-kill assay. Inhibitory effect of Cu-BTC (a) and Cu-GA (b) towards *E. coli* and *Lactobacillus*.

effect was found to be directly proportional to the concentration of both Cu-BTC and Cu-GA MOFs, with higher concentrations leading to more indistinct DNA bands.

Combining both Cu^{2+} and H_4gal within a framework facilitates sustained release, ensuring gradual infection inhibition. The framework gradually releases both the metal ion and organic linker, facilitating their attachement and internalization into the bacterial cell. Cu^{2+} ions and H_2gal^{2-} linkers disrupt bacterial cell membranes, causing leakage of cellular components and DNA damage, ultimately resulting in bacterial death. The possible mechanisms of both copper based MOFs are illustrated in Fig. 8. Our Cu-GA MOF capitalizes on the synergistic effects of both components. Also, we wanted to determine if the specificity of our Cu-GA MOF was due to the Cu^{2+} metal unit or the gallic acid linker. Our findings indicate that incorporating H_4gal enhances sensitivity towards Gram-negative bacteria. The metal unit is crucial for bacterial inhibition, and the H_2gal^{2-} linker may enable specific treatment of particular bacteria.

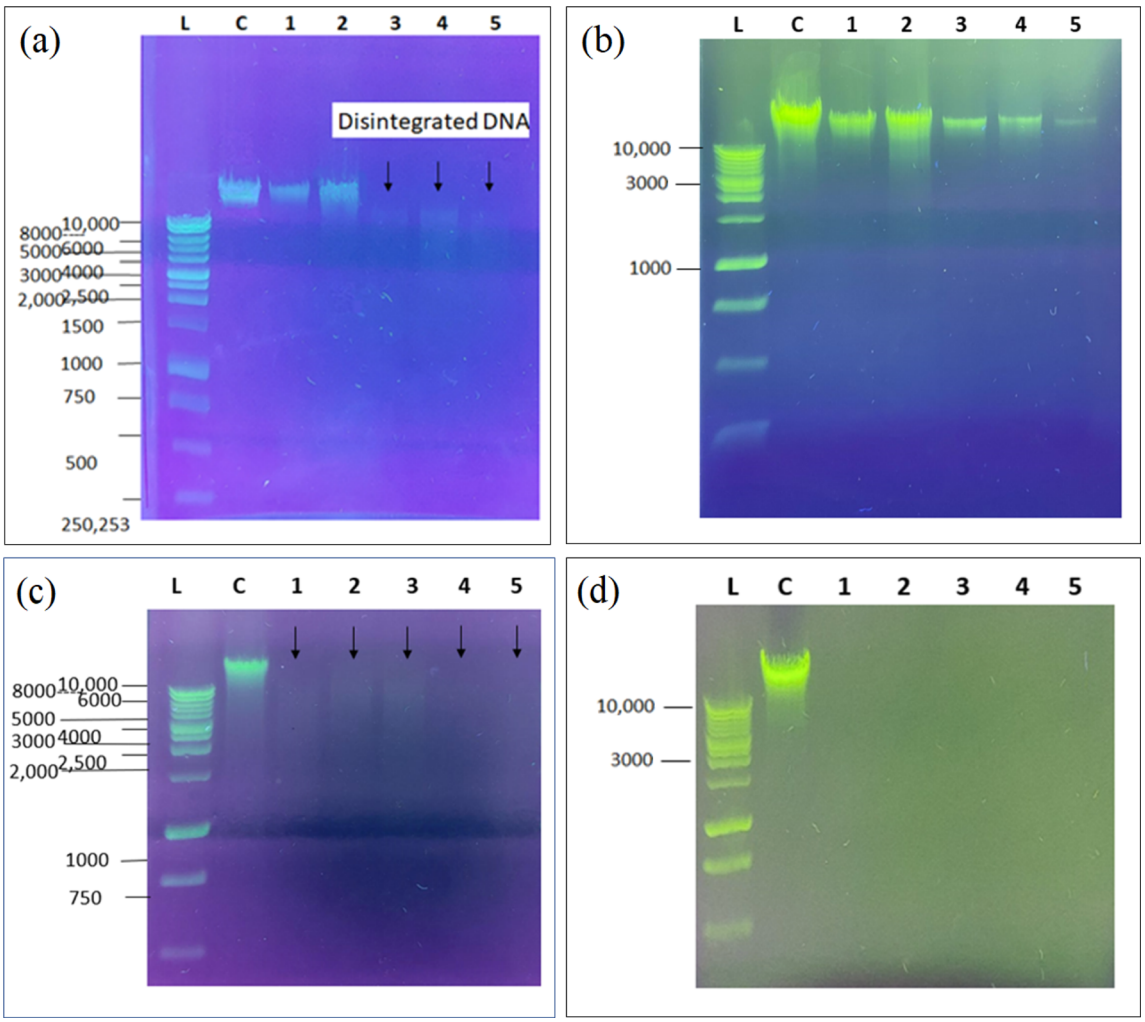

Fig. 7 DNA agarose gel electrophoresis of *E. coli* and *Lacobacillus* with Cu-BTC treatment (a and c) and Cu-GA treatment (b and d). L: 1kb DNA Ladder (Promega), C: control- E. coli DNA (without MOF treatment), 1: 0.125 × MIC, 2: 0.25 × MIC, 3: 0.5 × MIC, 4: 1 × MIC, 5: 1.5 MIC.

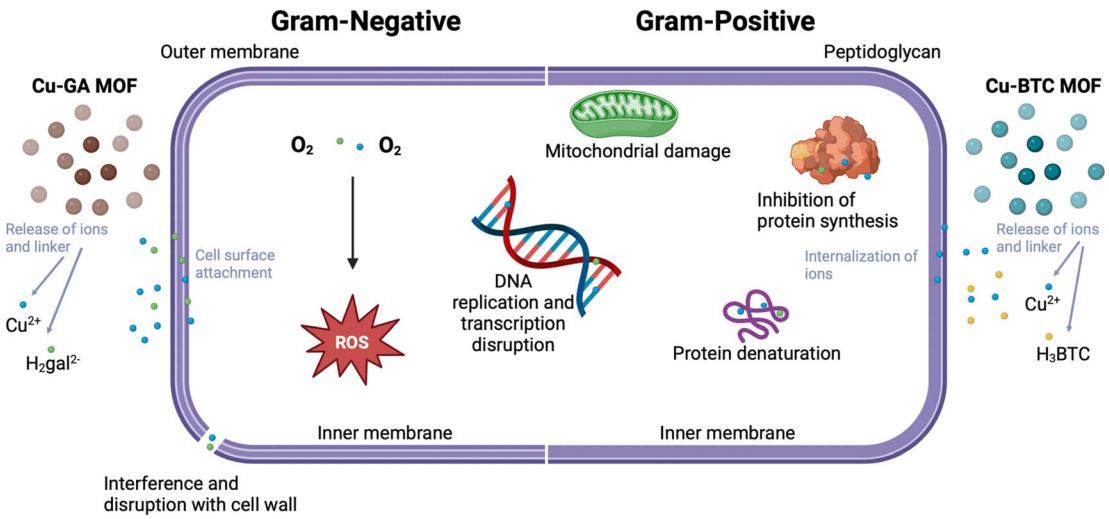

Fig. 8 Proposed antibacterial mechanisms of Cu-BTC and Cu-GA. Both MOFs release Cu^{2+} ions from their framework, facilitating their attachment and internalization on the surface of both Gram-negative and Gram-positive bacteria. In addition to Cu^{2+} ions, Cu-GA also releases H_2gal^{2-} from its framework, enhancing the antibacterial effect observed in *E. coli* (Gram-negative).

Conclusion

This study highlights the efficacy of Cu-BTC and Cu-GA as antibacterial agents, which have shown specificity and activity against two distinct types of bacterial strains. The mechanism by which these MOFs exert their antibacterial effect involves disrupting the cell membrane of *E. coli* and causing damage to bacterial DNA. The MOF treatment degrades the DNA of bacteria, which have already become vulnerable to the treatment by the destruction of their cell membrane. Cu-GA showed higher sensitivity against *E. coli*, possibly due to the presence of H_2gal^{2-} which can destroy the cellular membrane of bacteria. Conversely, Cu-BTC exhibited greater sensitivity against *Lactobacillus*. Both Cu-BTC and Cu-GA were effective in inhibiting the growth of Gram-positive and Gram-negative bacteria, which is a promising outcome in the face of increasing antibiotic resistance challenges. Advancements in nanoparticle systems have led to the targeted delivery of drugs, improving off-target effects and drug accumulation. MOFs for antibacterial treatment can be improved by adding targeting moieties to their surfaces, enhancing the overall efficacy and biodistribution. MOFs can also include current approved antibiotics, which could possibly restore or prevent the resistance of antibiotics against bacterial infections. Future development should focus more on the safety of metal-based nanoparticles. Surface modifications to improve MOF biocompatibility and biodegradability and how these modifications affect the release of MOF constituents should be explored.

Author contributions

Sandy Elmehrath: synthesis and characterization of the MOF structures, writing and proof-reading the manuscript. Khansa Ahsan: antibacterial assessment of the MOF structures. Nayla Munawar: supervising the antibacterial evaluation of the MOF structures. Ahmed Alzamly: characterization of the MOF structures. Ha L. Nguyen: characterization of the MOF structures, manuscript revision. Yaser Greish: planning of experiments, PhD Thesis advisor, funding of all experiments and characterization, proof-reading the final version of the manuscript.

Conflicts of interest

There are no conflicts to declare.

Acknowledgements

The authors acknowledge financial support from the UAEU research office and Zayed Centre for Health Sciences (ZCHS-UAEU) (Grants # 12R077 and 12R117).

References

1 H. Furukawa, *et al.*, The chemistry and applications of metal–organic frameworks, *Science*, 2013, **341**(6149), 1230444.
2 L. Jiao, J. Wang and H.-L. Jiang, Microenvironment modulation in metal–organic framework-based catalysis, *Acc. Mater. Res.*, 2021, **2**(5), 327–339.
3 W. Ni, *et al.*, Hierarchical MOF-on-MOF architecture for pH/GSH-controlled drug delivery and Fe-based chemodynamic therapy, *Inorg. Chem.*, 2022, **61**(7), 3281–3287.
4 K. Suresh and A. J. Matzger, Enhanced drug delivery by dissolution of amorphous drug encapsulated in a water unstable metal–organic framework (MOF), *Angew. Chem., Int. Ed.*, 2019, **58**(47), 16790–16794.
5 S. S. Dhankhar, N. Sharma and C. M. Nagaraja, Construction of bifunctional 2-fold interpenetrated Zn(II) MOFs exhibiting selective CO_2 adsorption and aqueous-phase sensing of 2,4,6-trinitrophenol, *Inorg. Chem. Front.*, 2019, **6**(4), 1058–1067.
6 H. Yu, *et al.*, Two highly water-stable imidazole-based Ln-MOFs for sensing Fe^{3+},Cr_2O7^{2-}/$CrO_4{}^{2-}$ in a water environment, *Inorg. Chem.*, 2020, **59**(3), 2005–2010.
7 W. Fan, *et al.*, Fine-tuning the pore environment of the microporous Cu-MOF for high propylene storage and efficient separation of light hydrocarbons, *ACS Cent. Sci.*, 2019, **5**(7), 1261–1268.
8 B. Chen, *et al.*, A microporous metal–organic framework for gas-chromatographic separation of alkanes, *Angew. Chem., Int. Ed.*, 2006, **45**(9), 1390–1393.
9 G. Zhou, *et al.*, Porphyrin–palladium hydride MOF nanoparticles for tumor-targeting photoacoustic imaging-guided hydrogenothermal cancer therapy, *Nanoscale Horizons*, 2019, **4**(5), 1185–1193.
10 F. Duan, *et al.*, Chromium-based metal–organic framework embedded with cobalt phthalocyanine for the sensitively impedimetric cytosensing of colorectal cancer (CT26) cells and cell imaging, *Chem. Eng. J.*, 2020, **398**, 125452.
11 A. P. Katsoulidis, *et al.*, Chemical control of structure and guest uptake by a conformationally mobile porous material, *Nature*, 2019, **565**(7738), 213–217.
12 A. C. Kathalikkattil, *et al.*, An lcy-topology amino acid MOF as eco-friendly catalyst for cyclic carbonate synthesis from CO_2: structure-DFT corroborated study, *J. Mater. Chem. A*, 2015, **3**(45), 22636–22647.
13 K. Huang, *et al.*, Photothermal hydrogel encapsulating intelligently bacteria-capturing bio-MOF for infectious wound healing, *ACS Nano*, 2022, **16**(11), 19491–19508.
14 W. Gao and L. Zhang, Nanomaterials arising amid antibiotic resistance, *Nat. Rev. Microbiol.*, 2021, **19**(1), 5–6.
15 S. Roy, I. Hasan and B. Guo, Recent advances in nanoparticle-mediated antibacterial applications, *Coord. Chem. Rev.*, 2023, **482**, 215075.
16 E. Cox, S. Nambiar and L. Baden, Needed: antimicrobial development, *N. Engl. J. Med.*, 2019, **380**(8), 783–785.
17 J. M. A. Blair, *et al.*, Molecular mechanisms of antibiotic resistance, *Nat. Rev. Microbiol.*, 2015, **13**(1), 42–51.
18 H. Huang, *et al.*, Advances in image-guided drug delivery for antibacterial therapy, *Adv. Drug Delivery Rev.*, 2023, **192**, 114634.

19 M. Rosenberg, *et al.*, Potential ecotoxicological effects of antimicrobial surface coatings: a literature survey backed up by analysis of market reports, *PeerJ*, 2019, **7**, e6315.
20 J. E. Stout and V. L. Yu, Experiences of the first 16 hospitals using copper-silver ionization for legionella control: implications for the evaluation of other disinfection modalities, *Infect. Control Hosp. Epidemiol.*, 2003, **24**(8), 563–568.
21 J. Harrison Joe, *et al.*, Copper and quaternary ammonium cations exert synergistic bactericidal and antibiofilm activity against *Pseudomonas aeruginosa*, *Antimicrob. Agents Chemother.*, 2008, **52**(8), 2870–2881.
22 S. A. Ibrahim, H. Yang and C. W. Seo, Antimicrobial activity of lactic acid and copper on growth of *Salmonella* and *Escherichia coli* O157:H7 in laboratory medium and carrot juice, *Food Chem.*, 2008, **109**(1), 137–143.
23 E. Santo Christophe, *et al.*, Contribution of copper ion resistance to survival of escherichia coli on metallic copper surfaces, *Appl. Environ. Microbiol.*, 2008, **74**(4), 977–986.
24 L. Weaver, H. T. Michels and C. W. Keevil, Survival of clostridium difficile on copper and steel: futuristic options for hospital hygiene, *J. Hosp. Infect.*, 2008, **68**(2), 145–151.
25 L. J. Wheeldon, *et al.*, Antimicrobial efficacy of copper surfaces against spores and vegetative cells of clostridium difficile: the germination theory, *J. Antimicrob. Chemother.*, 2008, **62**(3), 522–525.
26 G. Ren, *et al.*, Characterisation of copper oxide nanoparticles for antimicrobial applications, *Int. J. Antimicrob. Agents*, 2009, **33**(6), 587–590.
27 J. P. Ruparelia, *et al.*, Strain specificity in antimicrobial activity of silver and copper nanoparticles, *Acta Biomater.*, 2008, **4**(3), 707–716.
28 V. A. Gant, *et al.*, Three novel highly charged copper-based biocides: safety and efficacy against healthcare-associated organisms, *J. Antimicrob. Chemother.*, 2007, **60**(2), 294–299.
29 C. Carson Kerry, *et al.*, *In vitro* susceptibility of methicillin-resistant *Staphylococcus aureus* and methicillin-susceptible *Staphylococcus aureus* to a new antimicrobial, copper silicate, *Antimicrob. Agents Chemother.*, 2007, **51**(12), 4505–4507.
30 A. L. Casey, *et al.*, Role of copper in reducing hospital environment contamination, *J. Hosp. Infect.*, 2010, **74**(1), 72–77.
31 C. E. Santo, D. Quaranta and G. Grass, Antimicrobial metallic copper surfaces kill *Staphylococcus haemolyticus via* membrane damage, *MicrobiologyOpen*, 2012, **1**(1), 46–52.
32 L. Fang, *et al.*, Impact of cell wall structure on the behavior of bacterial cells in the binding of copper and cadmium, *Colloids Surf., A*, 2009, **347**(1), 50–55.
33 S. Langley and T. J. Beveridge, Effect of O-side-chain-lipopolysaccharide chemistry on metal binding, *Appl. Environ. Microbiol.*, 1999, **65**(2), 489–498.
34 D. Mitra, E.-T. Kang and K. G. Neoh, Antimicrobial copper-based materials and coatings: potential multifaceted biomedical applications, *ACS Appl. Mater. Interfaces*, 2020, **12**(19), 21159–21182.
35 J. A. Lemire, J. J. Harrison and R. J. Turner, Antimicrobial activity of metals: mechanisms, molecular targets and applications, *Nat. Rev. Microbiol.*, 2013, **11**(6), 371–384.
36 Y. N. Slavin, *et al.*, Metal nanoparticles: understanding the mechanisms behind antibacterial activity, *J. Nanobiotechnol.*, 2017, **15**(1), 65.
37 A. K. Chatterjee, R. Chakraborty and T. Basu, Mechanism of antibacterial activity of copper nanoparticles, *Nanotechnology*, 2014, **25**(13), 135101.
38 H. S. Rodríguez, *et al.*, Antibacterial activity against *Escherichia coli* of Cu-BTC (MOF-199) metal–organic framework immobilized onto cellulosic fibers, *J. Appl. Polym. Sci.*, 2014, **131**(19), 40815.
39 M. Su, *et al.*, *In situ* deposition of MOF199 onto hierarchical structures of bamboo and wood and their antibacterial properties, *RSC Adv.*, 2019, **9**(69), 40277–40285.
40 B. Ouyang, *et al.*, Low toxicity of metal–organic framework MOF-199 to bacteria *Escherichia coli* and *Staphylococcus aureus*, *J. Hazard. Mater. Adv.*, 2021, **1**, 100002.
41 O. Karimi-Khouzani, E. Heidarian and S. A. Amini, Anti-inflammatory and ameliorative effects of gallic acid on fluoxetine-induced oxidative stress and liver damage in rats, *Pharmacol. Rep.*, 2017, **69**(4), 830–835.
42 H. Rezaei-Seresht, *et al.*, Cytotoxic activity of caffeic acid and gallic acid against MCF-7 human breast cancer cells: an *in silico* and *in vitro* study, *Avicenna J. Phytomed.*, 2019, **9**(6), 574–586.
43 M.-S. Kang, *et al.*, Inhibitory effect of methyl gallate and gallic acid on oral bacteria, *J. Microbiol.*, 2008, **46**(6), 744–750.
44 Z.-J. Li, *et al.*, Antifungal activity of gallic acid *in vitro* and *in vivo*, *Phytother. Res.*, 2017, **31**(7), 1039–1045.
45 M. Inoue, *et al.*, Antioxidant, gallic acid, induces apoptosis in HL-60RG Cells, *Biochem. Biophys. Res. Commun.*, 1994, **204**(2), 898–904.
46 A. Li, *et al.*, Antibacterial activity of gallic acid from the flowers of *Rosa chinensis* Jacq. against fish pathogens, *Aquacult. Res.*, 2007, **38**(10), 1110–1112.
47 D. Shao, *et al.*, Inhibition of gallic acid on the growth and biofilm formation of *Escherichia coli* and *Streptococcus mutans*, *J. Food Sci.*, 2015, **80**(6), M1299–M1305.
48 A. Borges, M. J. Saavedra and M. Simões, The activity of ferulic and gallic acids in biofilm prevention and control of pathogenic bacteria, *Biofouling*, 2012, **28**(7), 755–767.
49 L. J. Nohynek, *et al.*, Berry phenolics: antimicrobial properties and mechanisms of action against severe human pathogens, *Nutr. Cancer*, 2006, **54**(1), 18–32.
50 H. Babich, *et al.*, Research strategies in the study of the pro-oxidant nature of polyphenol nutraceuticals, *J. Toxicol.*, 2011, **2011**, 467305.
51 Q. Wang, *et al.*, On mechanism behind UV-A light enhanced antibacterial activity of gallic acid and propyl gallate against *Escherichia coli* O157:H7, *Sci. Rep.*, 2017, **7**(1), 8325.
52 F. Enwa, Mechanisms of antimicrobial actions of phytochemicals against enteric pathogens – a review, *J. Pharm., Chem. Biol. Sci.*, 2014, **2**, 77–85.

53 K. Yang, *et al.*, Impact of gallic acid on gut health: focus on the gut microbiome, immune response, and mechanisms of action, *Front. Immunol.*, 2020, **11**.
54 A. S. F. T. A. Materials, *Standard Test Method for Determining the Antimicrobial Activity of Immobilized Agents under Dynamic Contact Conditions*, ASTM International, 2020.
55 C. Xu, *et al.*, Antibacterial activity and a membrane damage mechanism of Lachnum YM30 melanin against *Vibrio parahaemolyticus* and *Staphylococcus aureus*, *Food Control*, 2017, **73**, 1445–1451.
56 R. Moghimi, *et al.*, Investigations of the effectiveness of nanoemulsions from sage oil as antibacterial agents on some food borne pathogens, *LWT – Food Sci. Technol.*, 2016, **71**, 69–76.
57 J. Liu, *et al.*, Synthesis of chitosan-gallic acid conjugate: Structure characterization and *in vitro* anti-diabetic potential, *Int. J. Biol. Macromol.*, 2013, **62**, 321–329.
58 S. Sharma, *et al.*, Copper-gallic acid nanoscale metal–organic framework for combined drug delivery and photodynamic therapy, *ACS Appl. Bio Mater.*, 2019, **2**(5), 2092–2101.
59 B. Azhar, *et al.*, Aqueous synthesis of highly adsorptive copper–gallic acid metal–organic framework, *Sci. Rep.*, 2020, **10**(1), 19212.
60 A. K. Kar and R. Srivastava, An efficient and sustainable catalytic reduction of carbon–carbon multiple bonds, aldehydes, and ketones using a Cu nanoparticle decorated metal organic framework, *New J. Chem.*, 2018, **42**(12), 9557–9567.
61 D. Dorniani, *et al.*, Preparation of Fe_3O_4 magnetic nanoparticles coated with gallic acid for drug delivery, *Int. J. Nanomed.*, 2012, **7**, 5745–5756.
62 S. Shams, *et al.*, Cu/H_3BTC MOF as a potential antibacterial therapeutic agent against *Staphylococcus aureus* and *Escherichia coli*, *New J. Chem.*, 2020, **44**(41), 17671–17678.
63 S. S. Al Neyadi, *et al.*, UiO-66-NH_2 as an effective solid support for quinazoline derivatives for antibacterial agents against Gram-negative bacteria, *New J. Chem.*, 2021, **45**(43), 20386–20395.